



A strain-rate dependent material model for adipose tissue under blunt impact considering microstructural aspects

Felicitas Lanzl^{1,2}, Marcilio Alves³, Steffen Peldschus¹, Fabian Duddeck²

¹*Biomechanics and Accident Analysis, Institute of Legal Medicine, University of Munich
Nussbaumstr. 26, 80336, Munich, Germany*

felicitas.lanzl@med.uni-muenchen.de, steffen.peldschus@med.uni-muenchen.de

²*School of Engineering and Design, Technical University of Munich TUM
Arcisstr. 21, 80333, Munich, Germany*

duddeck@tum.de

³*Group of Solid Mechanics and Structural Impact, University of São Paulo*

Av. Prof. Mello Moraes 2231 São Paulo 05508-900 Brazil

maralves@usp.br

Abstract. Subcutaneous adipose tissue (SAT) is one of the superficial soft tissue layers covering the human body. Its mechanical behavior is important for various fields of impact biomechanics as it influences stresses and strains that are transferred to the underlying tissues. Modeling of SAT is challenging as it exhibits non-linear, strain rate and load case dependent characteristics. Here, we propose a new model of SAT under impact loading that considers microstructural aspects. The approach is based on a hyperelastic model whose strain energy function is split into a part for the incompressible lipid inside the cells and into a term for the collagen network encircling the spherical cells. Strain rate dependency is realized via a normalized relaxation function represented by a Prony series. The model is implemented as user defined material model into an FE code and used to simulate drop test experiments on porcine SAT specimens ($n = 12$) with varying thickness at an impact velocity of 1 m/s. The model has a stable and consistent behavior in the simulations. A reasonable match between experimental and simulation results is achieved for different specimen thicknesses, i.e. varying strain rates.

Keywords: subcutaneous adipose tissue, hyperelastic material modeling, strain rate dependency

1 Introduction

Next to skin and muscle tissue, subcutaneous adipose tissue (SAT) is one of the superficial soft tissues that form the outermost layers of the human body. Being the first layers that come into contact with a striking object during an impact they influence the stresses and strains that are transferred to subjacent tissues like bones or organs and, therefor also the injury risk of these underlying structures. Studies show that skin and subcutaneous tissue are able to absorb between 30 % up to 68 % of the impact energy in different impact scenarios [1, 2]. Thus, the mechanical behavior of SAT is important for various fields of impact mechanics, especially those that deal with the development of protective equipment. Whether it is for sport science to design innovative protectors or for automotive industry to develop new safety concepts for autonomous driving, considering the effect of subcutaneous adipose tissue enables to improve existing and derive novel solutions for the design of protective devices.

The microstructure of SAT basically consists of two main components - almost spherically shaped cells that are filled with an incompressible lipid, the so-called adipocytes, and the surrounding extracellular matrix, that is mainly comprised by collagenous structures [3, 4]. In both, humans and pigs, adipocytes have a diameter of approximately 80 μm and each adipocyte is encapsulated by a layer of collagen fibrils, with a thickness around 2 μm for porcine SAT [3, 5]. Due to the spherical shape of the adipocytes, this collagenous network, as a whole, exhibits the structure of a closed cell foam, which is referred to as *reinforced basement membrane* (RBM) throughout this work [5]. The second element of the extracellular matrix of SAT is depicted by long collagen fibers intervening the tissue space, similar to those in the dermis of the skin [3, 4]. According to Comley and Fleck [3], in porcine SAT those fibers can

be several millimeters in length, up to 30 μm thick and they form a three-dimensional network with no preferred orientation within the tissue. They are referred to as *septa fibers* (SF) throughout this work

Due to this intricate microstructure, SAT also displays complex material behavior featuring non-linear, strain rate as well as load case dependent characteristics. This makes material modeling of SAT a challenging task, especially for impact scenarios that involve combined loading, high tissue deformation and varying impact velocities. Up to now, most of the models used to depict SAT behavior under various loading conditions are hyperelastic models such as the Neo-Hookean model [6, 7], the Mooney-Rivlin model [7, 8], the Ogden model [5, 9] or the polynomial model [10]. However, those are phenomenological models that do not consider the microstructure of the material. Furthermore, most studies apply the models only in an analytical framework and do not include FE simulations. Apart from approaches that explicitly model the microstructural elements of SAT as different parts [11, 12], to the authors' knowledge, there is only one study investigating a microstructurally motivated model of SAT in the context of continuum mechanics. Sommer et al. [13] apply the Gasser-Ogden-Holzappel model [14] to depict SAT behavior under biaxial tension and simple shear. But this model focuses on the septa fibers rather than on the reinforced basement membrane as microstructural component of the SAT. Besides, the model is only examined under quasi static loading conditions and again, only in an analytical framework. Therefore, the object of this work is to develop a material model for SAT that (i) considers the microstructural aspects of SAT, especially the reinforced basement membrane, (ii) depicts strain rate dependent behavior, (iii) can be implemented into a FE environment and (iv) can be applied in the context of blunt impact scenarios, as now presented.

2 Material model

The material model, referred to as *circular fiber model* (CFM), is developed in the framework of hyperelastic material theory regarding SAT as a three-dimensional continuum. It is assumed that the strain energy function (SEF) of the model can be split into three different parts each one representing one microstructural element of the SAT. For a first version of the model, however, only the incompressible lipid inside the adipocytes and the reinforced basement membrane are considered. The volume fraction of the septa fibers in SAT is quite low, therefore it is assumed that its contribution to the bulk mechanical behavior is rather small compared to that of the reinforced basement membrane [3]. The general strain energy of the model thus reads:

$$\Psi_{CFM} = \Psi_{Lipid} + \Psi_{RBM}. \quad (1)$$

The strain energy function per unit volume representing the incompressible lipid Ψ_{Lipid} is modelled using a Neo-Hookean material [15], λ_i being the principal stretches in the three main directions and c is a material parameter with the dimension of stress:

$$\Psi_{Lipid} = \frac{c}{2}(\lambda_1^2 + \lambda_2^2 + \lambda_3^2 - 3). \quad (2)$$

The part of the strain energy per unit volume for the reinforced basement membrane Ψ_{RBM} is based on the fiber term in the Holzappel-Gasser-Ogden model [16]. It is hypothesized that the reinforced basement membrane consists of randomly, but equally distributed collagen fibers. It can then be simplified into three circular fiber families that encircle each adipocyte and are oriented in the three main planes of the global coordinate system. It is assumed that the contribution of each fiber family is equal and can be summed up to account for the material response of the complete reinforced basement membrane resulting in isotropic behavior. In contrast to linear fibers in the Holzappel-Gasser-Ogden model, these circular fibers not only depend on the stretch in one main direction, but on a combination of the stretch in two main directions representing the axes of the circular fiber as illustrated in Figure 1. The expression for the fiber stretch is based on the mathematical approximation for the perimeter of an ellipse. In addition, each circular fiber family only contributes to the mechanical behavior of the SAT if the circular fiber is under tension. Taking all these considerations into account, the strain energy function for the reinforced basement membrane becomes:

$$\Psi_{RBM} = \sum_{i=1}^3 \frac{1}{2} \frac{k_1}{k_2} [e^{k_2(\lambda_{CF,i}-1)^2} - 1]. \quad (3)$$

In this equation, k_1 depicts a material parameter with the dimensions of stress accounting for the strength of the reinforced basement membrane and k_2 is a dimensionless material parameter controlling the stiffening behavior of the circular fibers. The fiber stretch for each circular fiber (CF) family can be expressed by:

$$\lambda_{CF,1} = \begin{cases} 0.5(\lambda_1^2 + \lambda_2^2), & \text{if } \lambda_1^2 + \lambda_2^2 \geq 2 \\ 1, & \text{if } \lambda_1^2 + \lambda_2^2 < 2, \end{cases} \quad (4)$$

$$\lambda_{CF,2} = \begin{cases} 0.5(\lambda_2^2 + \lambda_3^2), & \text{if } \lambda_2^2 + \lambda_3^2 \geq 2 \\ 1, & \text{if } \lambda_2^2 + \lambda_3^2 < 2, \end{cases} \quad (5)$$

$$\lambda_{CF,3} = \begin{cases} 0.5(\lambda_1^2 + \lambda_3^2), & \text{if } \lambda_1^2 + \lambda_3^2 \geq 2 \\ 1, & \text{if } \lambda_1^2 + \lambda_3^2 < 2. \end{cases} \quad (6)$$

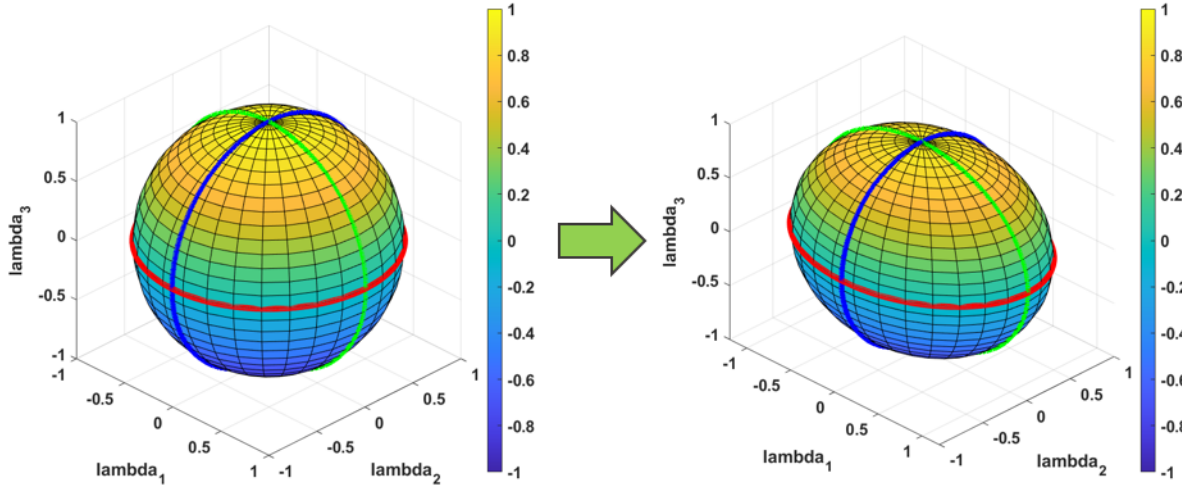


Figure 1. Deformation of the circular fibers does not only depend on the stretch in one main direction, but on a combination of the stretches in two main directions (circular fibers depicted in blue, red and green).

For implementation into an FE environment a volumetric and deviatoric decomposition of the model is performed using a formulation proposed by Ogden [17] with the volumetric term for the strain energy function given by:

$$\Psi_{vol} = \frac{\kappa}{81} [9 \ln(J) + (J)^{-9} - 1]. \quad (7)$$

J is the Jacobian determinant and κ is the bulk modulus of the material. Finally, strain rate dependency is introduced via a normalized relaxation function represented by a three-terms Prony series:

$$g(t) = \gamma_\infty \sum_{i=1}^3 \gamma_i e^{-\frac{t}{\tau_i}}. \quad (8)$$

t is the time, γ_∞ the normalized long term shear relaxation coefficient, γ_i the normalized shear relaxation coefficient of the i -th Prony term and τ_i the relaxation time of the i -th Prony term.

3 Methods

3.1 Drop test experiments

To investigate the influence of blunt force impact on SAT, drop test experiments are performed on $n = 12$ porcine SAT specimens. Samples consisting of skin, SAT and muscle tissue are resected from the abdomen of freshly slaughtered pigs and the skin and muscle tissue are carefully removed using a scalpel. Afterwards the excised SAT is trimmed with a custom built punch to obtain nearly rectangular specimens with a size of 50 mm x 50 mm. Specimen thickness is not changed and, thus, represents the original thickness of the SAT layer between skin and muscle tissue. Before each test, the thickness is measured with a caliper at three points of each specimen edge and an average thickness is calculated.

For the experiments, the specimens are placed on a steel ground plate (100 mm x 100 mm x 20 mm) with the side that was connected to the dermis before preparation facing towards the impactor. The impactor is a cylinder with an aluminum half-sphere (radius = 55 mm) on its end, which is guided in a drop tube device to achieve reproducible impact conditions. A uni-axial acceleration sensor with a range of ± 500 g (model 352C04, *PCB Piezotronics*, USA) is mounted centrally inside the impactor head to measure impactor acceleration during impact at a sampling rate of 50 kHz. Acceleration data is filtered using a SAE J211/1 low-pass filter at a channel frequency class of 600. Together, impactor and sensor exhibit a mass of 220 g. The drop height of the impactor can be continuously adjusted using an electromagnet and a drop height of 50 mm corresponding to an impact velocity of about 1 m/s is chosen for each test. Different strain rates are introduced due to the varying specimen thickness. Specimens are regularly moistened with 0.9 % sodium chloride solution during preparation and testing to avoid dehydration. A sketch of the experimental setup is depicted in Figure 2a.

In addition, 3D models of the specimens before and after impact are reconstructed using photogrammetry (*Agisoft PhotoScan*, version 1.1.4, *Agisoft LLC*, Russia). Therefore photographs of the specimen on the steel plate are taken from different views with a reflex camera (*Nikon AF-S DX Nikkor*, *Nikon*, Japan) using a rotatory table. A cube with an edge length of 10 mm is placed next to the SAT specimen and used dimensional reference for correct scaling of the models. Specimen thickness at the site of the impact is evaluated on the 3D reconstruction of each specimen using the software *3matics* (version 17.0, *Materialise GmbH*, Belgium).

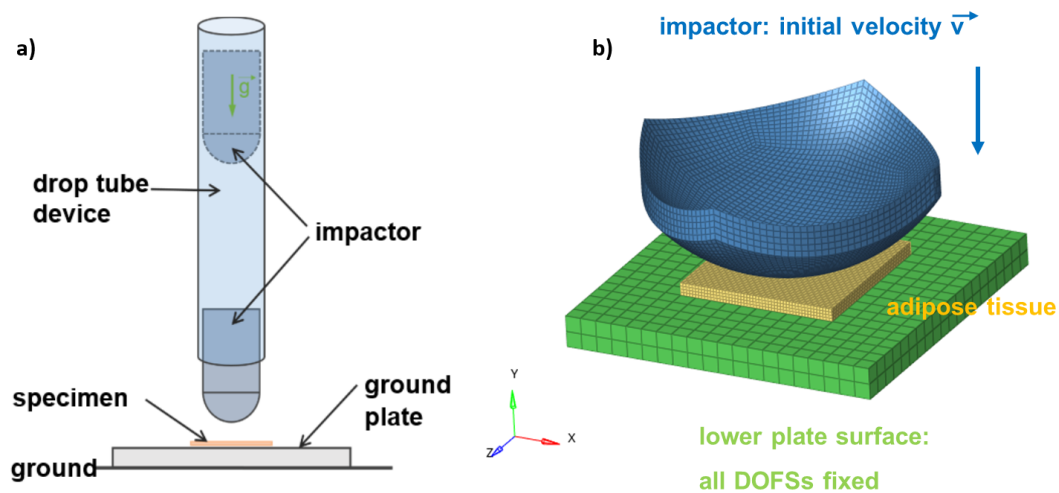


Figure 2. Sketch of the experimental drop test setup (a) and the associated FE model with applied boundary conditions (b).

3.2 Application of the material model in FE simulations

The circular fiber model presented in section 2 is implemented as user defined material model via a *FORTRAN 77* subroutine (*Intel Fortran Compiler*, version 18.0, *Intel Corporation*, USA) in the explicit FE code *VPS* (version 2019.0.3, *ESI group*, France). Then, the model is applied to simulate the drop test experiments described in section 3.1. Therefore, the main components of the experimental setup, i.e. impactor, specimen and ground plate, are transferred into an FE model using the software *Hypermesh* (version 2019.1, *Altair*, USA). All compo-

nents are represented by hexahedral elements and oriented according to the experiments. Plate and specimen are modeled as square blocks with an element size of 5 mm and 1 mm, respectively. Thickness of the specimen is varied between 5 mm and 8 mm according to the values evaluated for the experiments. To reduce computational cost, the impactor model only depicts the contact surface between impactor and specimen. It is modeled with an element size of 2 mm and an additional mass is added to achieve a final impactor mass of 220 g as in the experiments. An initial velocity of 1 m/s in negative y-direction is applied for all impactor nodes corresponding to the impact velocity in the experiments and all degrees of freedom are fixed for the nodes on the lower surface of the plate representing a fixed support. The complete setup is illustrated in Figure 2b.

A uniform reduced integration scheme in combination with hourglass control is employed for all components using a stiffness based hourglass control for the impactor and the plate and a viscous based hourglass control for the specimen. Contact interaction between the different parts is realized via symmetric node to segment contacts. Impactor and plate are modeled as ideal elastic-plastic materials with the material coefficients for aluminum and steel, respectively, whereas the circular fiber model is applied for the SAT specimen. Material and Prony series coefficients for the first simulation run are based on uniaxial compression data of porcine SAT by Comley and Fleck [5] at different strain rates and are adapted recursively to better match the experimental results. To compare simulation and experimental results, the time history of the impactor acceleration during simulation is evaluated by calculating the double derivative of the y-displacement of the impactor center node. As for the experiments, the acceleration data is filtered with a SAE J211/1 low-pass filter using a channel frequency class of 600. Evaluation of the experimental as well as the simulation results is performed in *Hypergraph* (version 2019.1, Altair, USA). All simulations are computed on two CPU cores (*Intel®Xeon®CPU E5-2650 v4, 2.20 GHz, Intel Corporation, USA*) using double precision.

4 Results and Discussion

Figure 3 shows a comparison of experimental and simulation results for the drop test setup. Four different specimen thicknesses (8 mm, 7 mm, 6 mm, and 5 mm), i.e. four different initial engineering strain rates (125 s^{-1} , 142.9 s^{-1} , 166.7 s^{-1} , 200 s^{-1}) are analyzed exemplarily. The range for the evaluated specimen thickness in the experiments lies between 4.8 mm and 8.3 mm. These values are based on the measurements of three-dimensional models reconstructed by photogrammetry as they are assumed to be more precise than the values resulting from the measurements with a caliper. Due to the softness of the SAT, its shape can easily be deformed by any manual handling, thus, introducing measurement errors, e.g. by too high compression between the tips of the caliper. Only one experimental result for a specimen thickness of 5 mm is available as specimen thickness has not been trimmed but rather represents the original thickness of the SAT layer between the skin and the muscle tissue of the excised sample. The maximum impactor acceleration determined in the experiments varies between 52.5 g and 80.7 g and increases with decreasing specimen thickness (see Figure 3). For all results, the loading phase of the acceleration response can be divided into two different parts - an initial part with a relatively low stiffness response followed by a second part with a rapid increase in stiffness. This reflects the non-linear material behavior of SAT that was also observed in other studies for various load cases, such as uniaxial compression, biaxial tension or simple shear [5, 13]. However, this division is not obvious for the acceleration response during the unloading phase that also exhibits a shorter duration in comparison to the loading phase. Total impact time decreases with decreasing specimen thickness, particularly, the initial shallow part of the loading phase becomes shorter for thinner specimens. In contrast, stiffness of the acceleration response increases for both parts of the loading phase for a reduced specimen thickness.

In general, simulation results show a good agreement with the experimental results for all investigated thickness values. The circular fiber model is able to reproduce the main characteristics of the experimental acceleration data quite well - the loading phase is separated into two parts with different stiffness increase and the unloading phase is shorter than the loading phase. Also in terms of impact time and acceleration values model performance is reasonable. However, acceleration response for a specimen thickness of 8 mm, 7 mm and 6 mm is too stiff in the initial part of the loading phase and maximum impactor acceleration for a specimen thickness of 5 mm is too high compared to the experimental results. A reason for this might be that the contribution of the septa fibers has not yet been included in the strain energy function of the model. Even though this contribution is supposed to be smaller than that of the reinforced basement membrane due to a lower volume fraction of the septa fibers compared to the reinforced basement membrane in the SAT [3], it may influence the material response of the SAT, especially at high deformation. Therefore, future work should include the implementation of a term representing the septa fibers in the SEF of the circular fiber model.

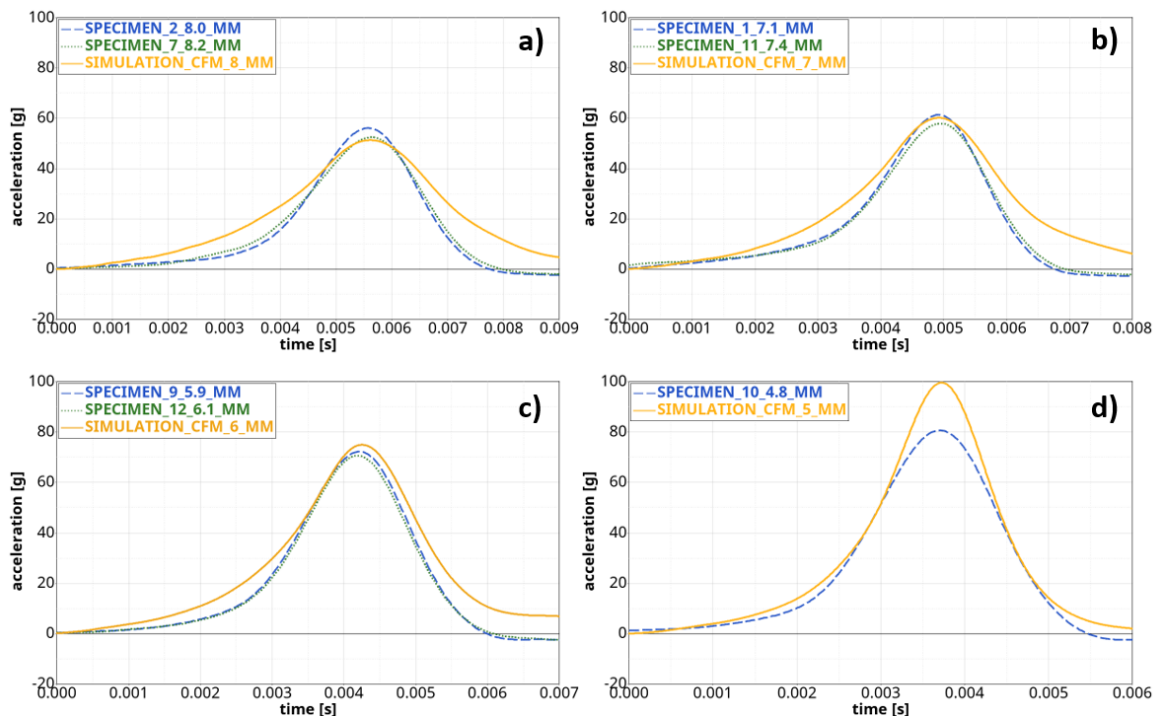


Figure 3. Comparison of experimental and simulation results for the drop test setup for different specimen thicknesses. a) 8 mm specimen thickness. b) 7 mm specimen thickness. c) 6 mm specimen thickness. d) 5 mm specimen thickness.

The material coefficients as well as the Prony series coefficients used as input for the final drop test simulations are listed in Table 1. But it has to be considered that these coefficients are evaluated based on experiments with porcine and not human SAT. Nevertheless, the main microstructural elements - lipid filled adipocytes, reinforced basement membrane and septa fibers - are the same for both, porcine and human SAT [3, 4] and the theory of the developed model is based on these elements. Thus, the model is expected to be also applicable for human SAT, although the material coefficients may be different in comparison to porcine SAT. In addition, only a limited range of strain rates is examined in this study. Implementation of additional Prony series terms might be necessary to depict a broader range of strain rates.

Table 1. Material and Prony series coefficients of the SAT material model used for the drop test simulations

| c | k_1 | k_2 | κ | γ_1 | τ_1 | γ_2 | τ_2 | γ_3 | τ_3 |
|-------|-------|-------|----------|------------|----------|------------|----------|------------|----------|
| [kPa] | [kPa] | [-] | [kPa] | [-] | [s] | [-] | [s] | [-] | [s] |
| 0.01 | 1.32 | 1.66 | 666.1 | 0.45 | 0.001 | 0.435 | 0.1 | 0.094 | 10.0 |

5 Conclusions

The strain energy function of the circular fiber model that is presented in this work is based on the specific microstructural elements of SAT and especially considers the reinforced basement membrane encircling the adipocytes as one of the main load bearing structures under deformation. The model also incorporates strain rate dependency via a normalized relaxation function that is represented by a three-terms Prony series. It can be implemented into an explicit FE environment and is able to reproduce the experimental response of porcine SAT in drop test experiments. Therefore, future work includes further examination of the model in various blunt impact scenarios, especially for a broader range of strain rates. Application of the model in more complex impact simulations comprising multi-layer compounds of skin and SAT or complete body parts, such as the head or the arm, is foreseen as a next step in this study. In addition, extension of the strain energy function by a third term representing the septa fibers of the SAT will be investigated.

Authorship statement. The authors hereby confirm that they are the sole liable persons responsible for the authorship of this work, and that all material that has been herein included as part of the present paper is either the property (and authorship) of the authors, or has the permission of the owners to be included here.

References

- [1] A. Trotta, D. Zouzias, G. Bruyne, and A. Ní Annaidh. The importance of the scalp in head impact kinematics. *Annals of Biomedical Engineering*, vol. 46, pp. 831–840, 2018.
- [2] V. Nikolić, J. Hančević, M. Hudec, and B. Banović. Absorption of impact energy in palmar soft tissues. *Anatomy and embryology*, vol. 148, pp. 215–221, 1975.
- [3] K. Comley and N. A. Fleck. A micromechanical model for the Young’s modulus of adipose tissue. *International Journal of Solids and Structures*, vol. 47, n. 21, pp. 2982–2990, 2010.
- [4] N. Alkhouli, J. Mansfield, E. Green, J. Bell, B. Knight, N. Liversedge, J. C. Tham, R. Welbourn, A. C. Shore, K. Kos, and C. P. Winlove. The mechanical properties of human adipose tissues and their relationships to the structure and composition of the extracellular matrix. *American Journal of Physiology-Endocrinology and Metabolism*, vol. 305, n. 12, pp. E1427–E1435, 2013.
- [5] K. Comley and N. Fleck. The compressive response of porcine adipose tissue from low to high strain rate. *International Journal of Impact Engineering*, vol. 46, pp. 1–10, 2012.
- [6] H. Naseri, H. Johansson, and K. Brolin. A Nonlinear Viscoelastic Model for Adipose Tissue Representing Tissue Response at a Wide Range of Strain Rates and High Strain Levels. *Journal of Biomechanical Engineering*, vol. 140, n. 4, pp. 041009–1–041009–8, 2018.
- [7] T. Payne, S. Mitchell, R. Bibb, and M. Waters. The evaluation of new multi-material human soft tissue simulants for sports impact surrogates. *J Mech Behav Biomed Mater*, vol. 41, pp. 336–356, 2015.
- [8] Y. Sun, L. Chen, lun K. Yick, W. Yu, N. Lau, and W. Jiao. Optimization method for the determination of Mooney-Rivlin material coefficients of the human breasts in-vivo using static and dynamic finite element models. *Journal of the Mechanical Behavior of Biomedical Materials*, vol. 90, pp. 615–625, 2019.
- [9] Z. Sun, S.-H. Lee, B. D. Gepner, J. Rigby, J. J. Hallman, and J. R. Kerrigan. Comparison of porcine and human adipose tissue loading responses under dynamic compression and shear: A pilot study. *Journal of the Mechanical Behavior of Biomedical Materials*, vol. 113, pp. 104112, 2021.
- [10] J. L. Calvo-Gallego, J. Domínguez, T. Gómez Cía, G. Gómez Ciriza, and J. Martínez-Reina. Comparison of different constitutive models to characterize the viscoelastic properties of human abdominal adipose tissue. a pilot study. *Journal of the Mechanical Behavior of Biomedical Materials*, vol. 80, pp. 293–302, 2018.
- [11] H. Ou, P. Zhan, L. Kang, J. Su, X. Hu, and S. Johnson. Region-specific constitutive modeling of the plantar soft tissue. *Biomechanics and Modeling in Mechanobiology*, vol. 17, pp. 1373–1388, 2018.
- [12] B. Seyfi, N. Fatourae, and A. Samani. A novel micro-to-macro structural approach for mechanical characterization of adipose tissue extracellular matrix. *Journal of the Mechanical Behavior of Biomedical Materials*, vol. 77, pp. 140–147, 2018.
- [13] G. Sommer, M. Eder, L. Kovacs, H. Pathak, L. Bonitz, C. Müller, P. Regitnig, and G. Holzapfel. Multiaxial mechanical properties and constitutive modeling of human adipose tissue: a basis for preoperative simulations in plastic and reconstructive surgery. *Acta Biomater*, vol. 9, pp. 9036–9048, 2013.
- [14] T. C. Gasser, R. W. Ogden, and G. A. Holzapfel. Hyperelastic modelling of arterial layers with distributed collagen fibre orientations. *Journal of The Royal Society Interface*, vol. 3, n. 6, pp. 15–35, 2006.
- [15] R. S. Rivlin and G. I. Taylor. Large elastic deformations of isotropic materials. i. fundamental concepts. *Philosophical Transactions of the Royal Society of London. Series A, Mathematical and Physical Sciences*, vol. 240, n. 822, pp. 459–490, 1948.
- [16] G. Holzapfel, T. Gasser, and R. Ogden. A new constitutive framework for arterial wall mechanics and a comparative study of material models. *Journal of Elasticity*, vol. 61, pp. 1–48, 2000.
- [17] R. W. Ogden. Large deformation isotropic elasticity: on the correlation of theory and experiment for compressible rubberlike solids. *Proceedings of the Royal Society of London*, vol. A328, pp. 567–583, 1972.